Available online at www.sciencedirect.com

ScienceDirect

journal homepage: http://www.elsevier.com/locate/rpor

Original research article

Local control rates in stereotactic body radiotherapy (SBRT) of lung metastases associated with the biologically effective dose

Daniel Zucca Aparicio[a,*], *Ovidio Hernando Requejo*[b], *Miguel Ángel de la Casa de Julián*[a], *Carmen Rubio Rodríguez*[b], *Pedro Fernández Letón*[a]

[a] *Servicio de Radiofísica y Protección Radiológica, Hospital Universitario HM Sanchinarro, Oña, 10, 28050 Madrid, Spain*

[b] *Servicio de Oncología Radioterápica, Hospital Universitario HM Sanchinarro, Oña, 10, 28050 Madrid, Spain*

ARTICLE INFO

Article history:
Received 7 May 2018
Accepted 2 January 2019
Available online 22 January 2019

Keywords:
SBRT
Local control
Biologically effective dose
Lung metastases

ABSTRACT

Aim: To evaluate dose differences in lung metastases treated with stereotactic body radiotherapy (SBRT), and the correlation with local control, regarding the dose algorithm, target volume and tissue density.

Background: Several studies showed excellent local control rates in SBRT for lung metastases, with different fractionation schemes depending on the tumour location or size. These results depend on the dose distributions received by the lesions in terms of the tissue heterogeneity corrections performed by the dose algorithms.

Materials and methods: Forty-seven lung metastases treated with SBRT, using intrafraction control and respiratory gating with internal fiducial markers as surrogates (*ExacTrac*, *BrainLAB AG*), were calculated using Pencil Beam (PB) and Monte Carlo (MC) (*iPlan*, *BrainLAB AG*).

Dose differences between both algorithms were obtained for the dose received by 99% ($D_{99\%}$) and 50% ($D_{50\%}$) of the planning treatment volume (PTV). The biologically effective dose delivered to 99% ($BED_{99\%}$) and 50% ($BED_{50\%}$) of the PTV were estimated from the MC results. Local control was evaluated after 24 months of median follow-up (range: 3–52 months).

Results: The greatest variations (40.0% in $\Delta D_{99\%}$ and 38.4% in $\Delta D_{50\%}$) were found for the lower volume and density cases. The $BED_{99\%}$ and $BED_{50\%}$ were strongly correlated with observed local control rates: 100% and 61.5% for $BED_{99\%} > 85$ Gy and <85 Gy ($p < 0.0001$), respectively, and 100% and 58.3% for $BED_{50\%} > 100$ Gy and <100 Gy ($p < 0.0001$), respectively.

* *Corresponding author.*
E-mail addresses: dzucca@hmhospitales.com (D.Z. Aparicio), ohernando@hmhospitales.com (O.H. Requejo), mdelacasa@hmhospitales.com (M.Á.d.l.C. de Julián), crubio@hmhospitales.com (C.R. Rodríguez), pfernandezleton@hmhospitales.com (P.F. Letón).

https://doi.org/10.1016/j.rpor.2019.01.001

Conclusions: Lung metastases treated with SBRT, with delivered $BED_{99\%} > 85$ Gy and $BED_{50\%} > 100$ Gy, present better local control rates than those treated with lower BED values ($p = 0.001$).

1. Background

The first treatments of pulmonary lesions using stereotactic body radiotherapy (SBRT) were described by Blomgren et al.[1] Since then, several published studies have shown excellent local control rates in hypofractionated treatments of lung metastases using SBRT, with different fractionation schemes and normalization depending on the location or size of the lesion.[2–14] The results of these series are associated with the dose distributions received by the lesions which are dependent on the tissue heterogeneity corrections performed by the dose algorithms. The research developed by De Jaeger et al.,[15] Chetty et al.,[16] and Lindsay et al.[17] are among the first to assess the influence of computational algorithms on improving clinical outcomes observed in patients treated for lung cancer.

2. Aim

The present work investigates the correlation between the biologically effective dose (BED) received by lung metastases treated with SBRT to the tumour control probability (TCP) to estimate the BED threshold above which successful local control rates are obtained. Likewise, the dosimetric differences found for each target, associated with the tissue heterogeneity corrections, were retrospectively evaluated to analyze their dependence on the volume and relative electron density for the planning treatment volume (PTV).

3. Materials and methods

3.1. *Cohort characteristics and radiation therapy technique*

The dosimetric results of a cohort of 29 patients with 47 lung metastases treated with SBRT were studied. Risk-adapted dose schemes based on published recommendations[18–20] were used according to the location of the lesion or proximity to critical structures, such as 10× 7.8 Gy (n = 5), 5 × 10 Gy (n = 12), 3 × 15 Gy (n = 4), 3 × 20 Gy (n=26).

Table 1 summarizes the tumours classified by volume and average electron densities of the PTV, enhancing the different dose prescription in terms of the BED ($\alpha/\beta = 10$ Gy for the tumour) to provide an overview of the cohort characteristics. In all the cases studied, the dose was prescribed to 95% of the target volume.

The maximum number of lesions treated per patient was one ($n = 20$), two ($n = 6$), four ($n = 1$), five ($n = 1$), and six ($n = 1$). For the patients with four, five and six metastases, the tumours were irradiated in several treatment courses, during a period of 27, 17 and 23 months, respectively. The anatomic distribution of the lesions was the right upper lobe (RUL) ($n = 10$), right middle lobe (RML) ($n = 6$), right lower lobe (RLL) ($n = 4$), left upper lobe (LUL) ($n = 13$), Lingula ($n = 2$), and left lower lobe (LLL) ($n = 12$).

Treatment plans performed on breath-hold computed tomography (CT) scans in exhale,[21] were based on 6–10 non-opposing coplanar static beams of 6 MV, with a median equivalent square of 34 mm (range: 23–63 mm), using a *Novalis* (BrainLAB AG, Feldkirschen, Germany), and delivered with the respiratory gating technique.[21] In each patient, an internal fiducial marker (*Visicoil Linear Fiducial Markers*, IBA Dosimetry, Germany) was implanted close to the target to correlate its movement with the respiratory cycle.

The markers were placed inside or near the lesion to be treated using the percutaneous technique, guided by CT.[22] If CT image artefacts are to be expected, their dosimetric impact can be mitigated by placing the markers near, but outside, the target volume. The use of implanted markers increases the accuracy of the system,[23,24] but, as a disadvantage, it requires an invasive procedure to introduce the markers, additionally complicated for patients with a decreased respiratory function. This procedure poses some associated risks, such as pneumothorax in the case of lung lesions.[25,26]

The management of the respiratory movement is performed with the aid of the ExacTrac system (Brainlab AG, Feldkirchen, Germany). At the start of each treatment session, the respiratory pattern of the patient is monitored for several cycles by means of a cluster of infrared reflectors placed on the skin before selecting a beam-on area. The setup corrections are automatically applied based on the position of the reflectors, using a couch with six degrees of freedom.[27] In this way, the treatment is delivered only when the reflectors are in the planned position from the simulation, within a certain tolerance.

The respiratory signal can be improved by placing additional reflectors on the diaphragmatic region. This platform incorporates a system of orthogonal stereoscopic X-ray images that allow to determine the position of the lesion by means of implanted markers or bony surrogates, during the active gate. It also allows the verification of the position of the target volume at any time during treatment.

The clinical target volume (CTV) was delineated in the lung and mediastinum windows. For the expansion of CTV-to-PTV, an isotropic margin of 2 mm was considered due to residual motion[28] of the tumour during the irradiation window (internal margin[29]), in addition to 3 mm for positioning uncertainties related to the radiological identification of the internal marker (setup margin[29]). The density used for the dose calculation was the original of the image study, i.e., no density override was performed.

Table 1 – Lung metastases distribution by volume and density attending to the dose prescription.

$n = 47$	Dose prescription (BED_p)							
	100 Gy		113 Gy		139 Gy		180 Gy	
	n	%	n	%	n	(%)	n	%
Total	12	25.5	4	8.5	5	10.6	26	55.3
Tumour volume (cm^3)								
<10	3	6.4	2	4.3	0	0.0	8	17.0
10–20	3	6.4	2	4.3	1	2.1	13	27.7
20–30	3	6.4	0	0.0	1	2.1	1	2.1
30–40	1	2.1	0	0.0	1	2.1	0	0.0
40–50	1	2.1	0	0.0	1	2.1	3	6.4
50–60	0	0.0	0	0.0	0	0.0	0	0.0
60–70	0	0.0	0	0.0	1	2.1	0	0.0
70–80	0	0.0	0	0.0	0	0.0	0	0.0
80–90	0	0.0	0	0.0	0	0.0	1	2.1
>90	1	2.1	0	0.0	0	0.0	0	0.0
Tumour density (ρ_e^w)								
<0.1	0	0.0	0	0.0	0	0.0	0	0.0
0.1–0.2	0	0.0	0	0.0	0	0.0	1	2.1
0.2–0.3	1	2.1	0	0.0	0	0.0	5	10.6
0.3–0.4	1	2.1	1	2.1	0	0.0	7	14.9
0.4–0.5	2	4.3	3	6.4	1	2.1	5	10.6
0.5–0.6	2	4.3	0	0.0	2	4.3	1	2.1
0.6–0.7	4	8.5	0	0.0	1	2.1	2	4.3
0.7–0.8	1	2.1	0	0.0	0	0.0	4	8.5
0.8–0.9	1	2.1	0	0.0	1	2.1	1	2.1
>0.9	0	0.0	0	0.0	0	0.0	0	0.0

BED_p: biologically effective dose prescribed; ρ_e^w : average electron density.

The radiotherapy treatment planning system (TPS) used in our study was *iPlan RT Dose* (BrainLAB AG, Feldkirschen, Germany). The lesions treated between April 2008 and April 2011 were calculated using the Pencil Beam (PB) algorithm. Since then, the calculation algorithm used has been Monte Carlo (MC) (XVMC code[30–36]). The superiority of the MC algorithm compared to PB is well established in the literature, specifically in low density media.

Nevertheless, as PB has long been used for clinical purposes at our institution during, it is of concern to compare the treatment plans calculated with both dose engines in order to achieve a relationship of the dose discrepancies with the clinical outcome. For this reason, 30 cases originally calculated with PB were recalculated for this study with MC, while 17 cases clinically planned with MC have been recalculated with PB, for comparison purposes. The same beam arrangement and monitor units (MU) for each field were preserved.

To compensate for the dose reduction on the target obtained with MC compared to PB, there are several strategies such as increasing the beam dimensions to consider an additional margin accounting for the increased penumbra found with MC, or generate small segments in the sub-dosage zones to increase the dose or normalize the dose by increasing the coverage values at the expense of a hotspot presence in the central region of the lesion, provided that they do not cause a risk for the patient and the dose is accurately delivered to the tumour.

3.2. *Influence of the dose calculation algorithm, volume and density of the tumour*

The dose deviation between MC and PB, normalized to the prescription dose $(D_{MC} - D_{PB})/D_p$, has been evaluated for the dosimetric indicators, near-minimum dose ($D_{99\%}$) and median dose ($D_{50\%}$) for the PTV. For this purpose, the dose–volume histograms (DVH) obtained for each dose algorithm were sampled with a resolution of 1.0 mm and 0.5% of the prescription dose, from TPS to a spreadsheet that was used for analyzing the set of cases.

For dose calculation with PB, a spatial resolution of 3.0 mm was used. The same resolution for MC implies an internal calculation grid size of 2.6 mm × 2.6 mm × 3.0 mm, since the dimensions of each voxel from the CT study are 0.9 mm × 0.9 mm × 3.0 mm. In addition, a mean variance of 1.0% and dose-to-medium (D_M) were considered as MC calculation parameters.

For pulmonary lesions, there is agreement between D_M and dose-to-water (D_W), since the unrestricted stopping-power ratio water to lung is approximately 1.0 in the energy range of 6 MV.[37] The dosimetric indicators $D_{99\%}$ and $D_{50\%}$ calculated with MC were compared to PB, while the normalized dose deviations between both algorithms, $\Delta D_{99\%}$ and $\Delta D_{50\%}$, were fitted to the inverse of the volume and to the average electron density relative to water for the PTV by means of linear regression.

3.3. *Influence of the biologically effective dose on the tumour control probability*

Patient follow-up consisted of tumour review using CT or PET-CT imaging every three months for the first two years, every six months during the following year, and at the discretion of the physician thereafter. Local control was established as the stability or reduction of the tumour volume without progression during follow-up.

The dose received by 99% and 50% of the PTV volume, $D_{99\%}$ and $D_{50\%}$ respectively, and calculated with MC for each target, were converted according to the fractionation schemes to $BED_{99\%}$ and $BED_{50\%}$ ($\alpha/\beta = 10$ Gy for the tumour).

From the contingency tables that represent the true positive and negative rates, in addition to false positive and negative rates, according to that local control for the PTV was achieved or not, for a given threshold value of the $BED_{99\%}$ and $BED_{50\%}$, the construction of the ROC curves (*Receiver Operating Characteristic*) could be performed.[38]

The related local control rates were calculated for the different $BED_{99\%}$ and $BED_{50\%}$ received by the PTV. Tumour control probabilities based on the delivered $BED_{99\%}$ and $BED_{50\%}$ were obtained, adjusting the local control data experimentally observed by means of Origin 7.0 (*OriginLab Corporation*, Northampton, MA), and following the model of TCP described by Kallman et al.[39] for a cell damage model based on Poisson

Table 2 – Analysis of the dose–volume deviation attending to dose calculation algorithm, volume and density of the PTV.

$n = 47$	Deviation of the dose–volume parameters for the PTV: $(D_{MC} - D_{PB})/D_p$					
	$\Delta D_{99\%}$			$\Delta D_{50\%}$		
	n	%	p-Value	n	%	p-Value
Range			0.0003			<0.0001
0–5%	3	6.4		4	8.5	
5–10%	6	12.8		17	36.2	
10–15%	11	23.4		10	21.3	
15–20%	10	21.3		10	21.3	
20–25%	6	12.8		2	4.3	
25–30%	7	14.9		1	2.1	
30–35%	2	4.3		2	4.3	
35–40%	1	2.1		1	2.1	
40–45%	1	2.1		0	0.0	
Accumulated						
<10%	9	19.1		21	44.7	
<15%	20	42.6		31	66.0	
<20%	30	63.8		41	87.2	

	Multiple linear regression analysis					
	$D_{99\%\ PB}$ Slope	ρ_e^w Slope	Volume^{-1} Slope	y-Intercept	r	p-Value
$D_{99\%\ MC}$	0.655			0.172	0.508	0.0003
95% CI	0.321–0.988			−0.166 to 0.509	0.259–0.694	
$\Delta D_{99\%}$		0.359		−0.355	0.718	<0.0001
95% CI		0.255–0.464		−0.410 to 0.300	0.543–0.833	
$\Delta D_{99\%}$			−0.854	−0.102	0.658	<0.0001
95% CI			−1.148 to 0.561	−0.135 to 0.069	0.457–0.795	
$\Delta D_{99\%}$		0.371	0.007	−0.372	0.719	<0.0001
95% CI		0.243–0.500	−0.036 to 0.050	−0.490 to 0.253	0.544–0.834	

	Multiple linear regression analysis					
	$D_{50\%\ PB}$ Slope	ρ_e^w Slope	Volume^{-1} Slope	y-Intercept	r	p-Value
$D_{50\%\ MC}$	0.659			0.238	0.561	<0.0001
95% CI	0.367–0.951			−0.079 to 0.555		
$\Delta D_{50\%}$		0.399		−0.328	0.850	<0.0001
95% CI		0.325–0.473		−0.367 to 0.289		
$\Delta D_{50\%}$			−1.018	−0.042	0.837	<0.0001
95% CI			−1.218 to 0.818	−0.064 to 0.019		
$\Delta D_{50\%}$		0.370	−0.017	−0.287	0.855	<0.0001
95% CI		0.279–0.460	−0.047 to 0.013	−0.370 to 0.204		

D_p: dose prescribed; $\Delta D_{99\%}$: dose differences for the 99% of the PTV; $\Delta D_{50\%}$: dose differences for the 50% of the PTV; ρ_e^w : average electron density; CI: confidence interval.

statistics in which D_{50} represents the dose for which a control rate of 50% is obtained and γ_{50} is the normalized-slope of the sigmoid dose–response curve for the D_{50}.

3.4. Statistical analysis and endpoints

The *Pearson* correlation coefficients and the 95% confidence intervals (95% CI) for the linear regression analysis were obtained using the *Excel 2013* statistical tools (*Microsoft Corporation*, Redmond, WA). Statistical significance was determined using the two-tailed *Student's t*-test. The thresholds for $BED_{99\%}$ and $BED_{50\%}$, obtained from the ROC curves, served as prognostic factors for the local control rates related to the follow-up by means of the Kaplan–Meier analysis,[40] developed using *SPSS Statistics 20.0* (IBM, Armonk, NY).

4. Results

4.1. Influence of the dose calculation algorithm, volume and density of the tumour

The deviations between both calculation algorithms were statistically significant ($p < 0.001$, *Wilcoxon* signed-rank test) and greater than 20% for $\Delta D_{99\%}$ in 36.2% of the cases and in 12.8% for the $\Delta D_{50\%}$. The greatest deviations (40.0% in $\Delta D_{99\%}$ and 38.4% in $\Delta D_{50\%}$) were found for very small lesions or isolated in the middle of lung tissue.

Table 2 summarizes the results of the linear regression analysis found for the dose calculated with MC respect to PB, as well as the deviations between both dose algorithms as a function of the inverse of the volume and the average electron density of the PTV. The *Pearson* correlation coefficients are represented, in addition to the corresponding 95% confidence intervals.

The discrepancies between algorithms, $\Delta D_{99\%}$ and $\Delta D_{50\%}$, are inversely proportional to the volume and the average electron density of the PTV (Fig. 1). The greatest deviations are found for the cases of lower density, where the tumour is practically equivalent to lung tissue, which in general, agree with the cases of lower volume, due to the greater proportion within the PTV of lung density surrounding the boundary of the CTV with soft-tissue density. The correlation between volume and density of PTV was statistically significant ($r = 0.655$, $p < 0.001$).

4.2. Influence of the biologically effective dose on the tumour control probability

After a median follow-up of 24 months (range: 3–52 months), five metastases had local recurrence within the group of lesions originally treated with PB ($n = 30$; 83.3% crude local control rate). These recurrences were observed after a median of 9 months subsequent to the treatment. For this group of lesions, local progression rates of 13.0% to 9 months, 18.5% to 18 months and 30.1% to 35 months were estimated. Within the group of lesions originally calculated with MC, no local recurrence was observed ($n = 17$, 100% local control rate), after a median follow-up of 23 months (range: 3–31 months).

Although the comparison between algorithms, regarding local recurrence rates, is not statistically significant ($p = 0.115$, *log-rank* test), a clear difference in local control rates between algorithms is found beyond the ninth month after treatment (70% for PB versus 100% for MC).

For the cases originally planned with PB, the $BED_{99\%}$ and $BED_{50\%}$ were recalculated with MC. These values were systematically lower than the BED prescribed, due to the inaccuracies of the PB calculation in low density media and small fields, which lead to a loss of coverage and a reduction of the $D_{99\%}$ and $D_{50\%}$.

The $BED_{99\%}$ and $BED_{50\%}$ closer to the prescribed BED, and actually received by the PTV, are those calculated with MC. The temporal evolution of the BED received by the tumours shows a gap at the time when the MC algorithm was implemented (Fig. 2). The difference between the BED values calculated before and after this moment, assuming unequal variances, is statistically significant ($p < 0.0001$, two-tailed *Student's t*-test) for both $BED_{99\%}$ and $BED_{50\%}$.

The areas under the ROC curves (AUC) were 0.938 (95% CI: 0.859–1000, $p < 0.002$) and 0.929 (95% CI: 0.850–1000, $p < 0.002$) for the $BED_{99\%}$ and $BED_{50\%}$, respectively. The dose received by the lesion was relevant to obtain an adequate local control. For the $BED_{99\%}$, a cut-off dose of 85 Gy was established, for which local control rates of 100% and 61.5% were found for cases above and below this threshold ($p < 0.0001$), respectively.

In the case of the $BED_{50\%}$, the established cut-off dose was 100 Gy, for which local control rates of 100% and 58.3% were found for cases above and below this threshold ($p < 0.0001$), respectively. The dependence between the BED threshold and local control is statistically significant ($p = 0.001$, two-tailed *Fisher's F*-test).

The TCP curves adjusted experimentally based on the BED received by the tumours of this study show that the D_{50} were $50.91\,Gy \pm 1.51\,Gy$ and $58.08\,Gy \pm 2.68\,Gy$ for $TCP_{99\%}$ and $TCP_{50\%}$, respectively, whereas the slopes, γ_{50}, were 0.60 ± 0.08 and 0.53 ± 0.10, respectively (Fig. 3). Actuarial local control rates for $BED_{99\%} < 85\,Gy$ were 72.7% at 9 months, 62.3% at 18 months and 49.9% at 35 months ($p < 0.002$, *log-rank* test), respectively, whereas for $BED_{50\%} < 100\,Gy$ were 70.0% at 9 months, 58.3% at 18 months and 43.7% at 35 months ($p < 0.001$, *log-rank* test), respectively (Fig. 4).

5. Discussion

In the present work, the dosimetric differences found for lung metastases treated with SBRT, owing to the heterogeneity corrections of dose algorithm, were retrospectively evaluated to analyze also their dependence on the volume and relative electron density of the PTV. The variation of dosimetric indicators due to dose algorithm increases as the volume and density of the lesion are reduced, since the radiation fields are smaller, and the presence of low density tissue heterogeneity associated with the lung environment produces a lack of lateral electronic equilibrium[41] causing a reduction of the dose, mainly in the tumour–lung interface.

This phenomenon is not accurately considered in the PB algorithm, causing an overestimation of the absorbed dose compared to MC. In addition, this effect produces a substantial dose heterogeneity in the PTV, with a lack of coverage that cannot be compensated simply by rescaling the

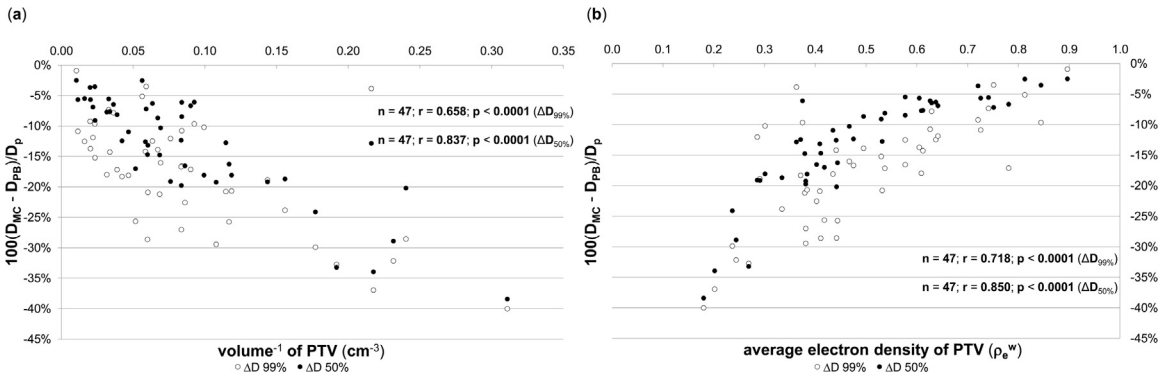

Fig. 1 – Dose–volume deviations between Monte Carlo (D_{MC}) and Pencil Beam (D_{PB}), normalized to the prescription dose (D_p), received by 99% and 50% of the planning target volume (PTV), $\Delta D_{99\%}$ and $\Delta D_{50\%}$ respectively, regarding: (a) the inverse value of the target volume and (b) the average electron density.

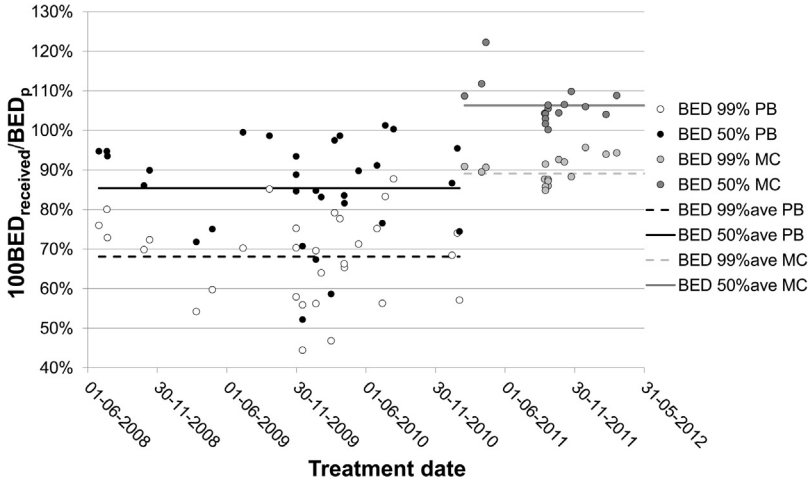

Fig. 2 – Temporal evolution of the biologically effective dose (BED), and the averaged value (horizontal lines), received by 99% and 50% of the PTV. The use of the MC dose algorithm on 2011 is shown as a gap. $BED_{99\%\ PB}$ and $BED_{50\%\ PB}$ are the BED recalculated with MC for the plans originally calculated and delivered with the PB algorithm, while $BED_{99\%\ MC}$ and $BED_{50\%\ MC}$ represent the BED for the plans actually calculated and delivered with the MC dose distribution.

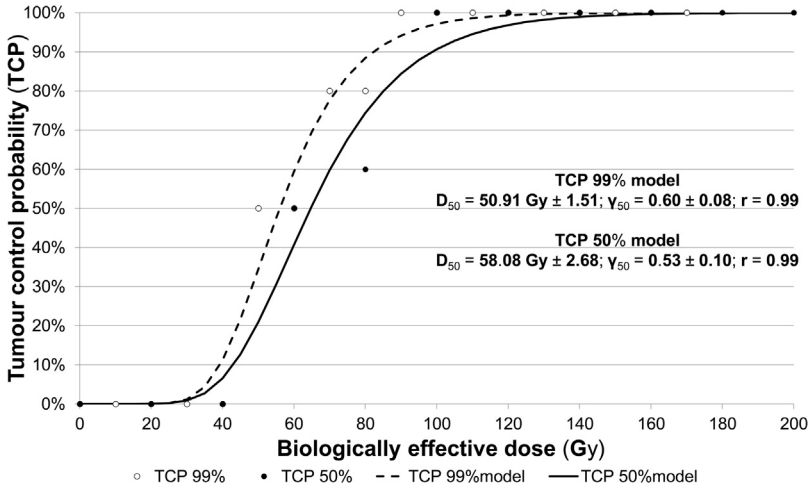

Fig. 3 – Tumour control probabilities (TCP) found for the BED received by 99% and 50% of the PTV, $BED_{99\%}$ and $BED_{50\%}$ respectively. Dashed and solid lines represent the TCP models that best fit to the achieved results.

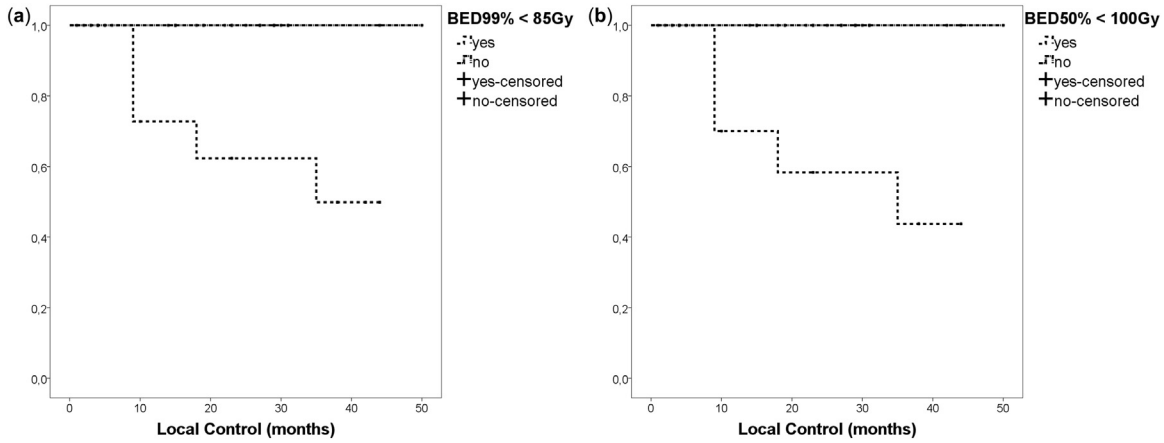

Fig. 4 – Local control rates found for (a) the BED received by 99% and (b) 50% of the PTV. $BED_{99\%} > 85$ Gy and $BED_{50\%} > 100$ Gy are correlated to better local control rates than those treated with lower BED values ($p = 0.001$).

dose calculated with MC, without the appearance of hot-spots inside the target. These discrepancies are as much greater as smaller become the dimensions of the lesion, as usually is the case with the SBRT treatments, since the ratio between the surface and the volume of the lesion increases with the reduction of the tumour volume, thus giving more relevance to the surface effects.[42]

The differences between MC and PB depend on the arrangement of the beams, dimensions of the fields, energy, size and location of the tumour, particularly in anatomical sites where the target is close to tissues with very variable densities, such as the lung or head and neck. All these factors make it challenging to predict the actually delivered dose distribution from the PB calculation. Our results show a great dispersion, since the location of the lesion inside the lung is relevant, regardless of its volume, considering that treatment beams for lesions close to the mediastinum or chest wall will follow different radiological paths.

Other authors[43–47] have presented similar results to our work for different fractionation schemes, where the greatest differences between dose algorithms were found for the smaller lesions, embedded in lung tissue, thus the doses received by the tumour were highly dependent on the size, tissue density and location. In all cases, the dose calculated by PB was higher than that obtained by algorithms with adequate heterogeneity correction as MC or *Acuros XB*.

Dose escalation is an essential issue for establishing the most adequate fractionation scheme for achieving a successful tumour control,[48] minimizing the likelihood of adverse treatment-related side effects. However, it is difficult to compare the results given the variability of fractionation schemes, in addition to the differences in the normalization of the prescription doses, which are not always reported in the published works.

In contrast to a study presented by Xiao et al.,[49] where they suggested to prescribe 18 Gy instead of 20 Gy per fraction, for treatments calculated using convolution-superposition algorithms, and following the recommendations of RTOG 0236[50] guidelines that explicitly excluded heterogeneity corrections, the study of Zhuang et al.[44] indicated that a simple rescaling would not be enough to compensate for the differences due to these corrections, given the strong dependence observed in the volume and location of the lesions considered in their study. This argument reinforces our approach to this scenario by generating segments of small dimensions in the sub-dosing zones to increase the dose at the edge of the PTV for achieving satisfactory coverage values.

Regarding the tumour control associated with the BED received by the lesions of our cohort, we established a $BED_{99\%}$ cut-off value of 85 Gy with local control rates at 35 months of 100% and 49.9% for the cases above and below this threshold ($p < 0.002$), respectively, and a $BED_{50\%}$ cut-off value of 100 Gy with local control rates at 35 months of 100% and 43.7% for the cases above and below this threshold ($p < 0.001$), respectively. The detriment found due to the change in dose algorithm has been manifested especially in a lack of coverage at the edges of the PTV. In this sense, the parameter $D_{99\%}$ was more sensitive to changes than $D_{50\%}$.

These results are linked to those found by Guckenberger et al.[51,52] who showed lower BED values received by 95% of the PTV ($BED_{95\%}$) generated from an ITV plus a symmetric margin of 5 mm, calculated by 3D dosimetry with heterogeneity correction, compared to the $BED_{95\%}$ of the CTV calculated by 4D dosimetry on imaging studies acquired in 8 phases of the respiratory cycle and using deformable registration for the accumulation of the dose.

The hazard ratio cannot be calculated because all cases evaluated were censored owing to no relapse in the groups of higher doses. For this reason, our results are clearly better than those published by other studies and superimposable to those obtained by Rusthoven et al.[12] in the phase I/II study.

The relationship between tumour control and the BED received by the lesion has also been analyzed by Guckenberger et al.[52] who obtained a $BED_{95\%}$ cut-off values of 80 Gy for the 3D dosimetry calculated on the PTV and of 100 Gy for the 4D dosimetry calculated on the CTV with significantly higher local control rates for the cases above these thresholds.

The dose–response curve exhibits a *plateau* around the BED of 100 Gy. Whenever the dose reduction calculated with appropriate heterogeneity correction still provides a BED > 100 Gy,

the TCP will remain suitable. In general, the results published for local control[3–5,9,10,53,54] are better in the hypofractionated treatments based on fractionation schemes with a BED > 100 Gy. Dose differences in the order of 5% to 10% related to the calculation algorithm may be clinically detectable, in addition to producing changes in the TCP from 10% to 20%, or changes in the normal tissue complications probability (NTCP) from 20% to 30%.[55]

6. Conclusions

A prognostic factor for the local control is the delivered dose. The BED delivered with Monte Carlo is significantly greater than those received with Pencil Beam, while there is no statistically significant dependence between the local control and the dose algorithm used.

With the fractionation schemes used in our study, we obtained that targets receiving $BED_{99\%} > 85$ Gy or $BED_{50\%} > 100$ Gy, present significantly better local control rates than those treated with lower BED values ($p = 0.001$). These cut-off BED values were obtained for lung metastases treated with SBRT, using intrafraction control and the respiratory gating technique, but they could also be of broader applicability to other clinical scenarios.

Authors' contributions

DZA performed the retrospective analysis of the dose deviation for the lung tumours due to calculation algorithm, BED and TCP evaluation, and was a major contributor in writing the manuscript. OHR analyzed and interpreted the patient data regarding the local control, and made substantial contributions to acquisition of data, MAC collaborated to the analysis and interpretation of the results and the discussion, and PFL suggested the conception of this study; OHR, MAC, CRR and PFL have revised the manuscript, besides to provide intellectual content. All authors have read and approved the final manuscript.

Conflict of interest

None declared.

Financial disclosure

None declared.

REFERENCES

1. Blomgren H, Lax I, Naslund I, Svanstrom R. Stereotactic high dose fraction radiation therapy of extracranial tumours using an accelerator. Clinical experience of the first thirty-one patients. *Acta Oncol* 1995;**34**:861–70.
2. Uematsu M, Shioda A, Tahara K, et al. Focal, high dose, and fractionated modified stereotactic radiation therapy for lung carcinoma patients: a preliminary experience. *Cancer* 1998;**82**:1062–70.
3. Nagata Y, Negoro Y, Aoki T, et al. Clinical outcomes of 3D conformal hypofractionated single high-dose radiotherapy for one or two lung tumours using a stereotactic body frame. *Int J Radiat Oncol Biol Phys* 2002;**52**:1041–6.
4. Nakagawa K, Aoki Y, Tago M, Terahara A, Ohtomo K. Megavoltage CT-assisted stereotactic radiosurgery for thoracic tumours: original research in the treatment of thoracic neoplasms. *Int J Radiat Oncol Biol Phys* 2000;**48**:449–57.
5. Hara R, Itami J, Kondo T, et al. Stereotactic single high dose irradiation of lung tumours under respiratory gating. *Radiother Oncol* 2002;**63**:159–63.
6. Whyte RI, Crownover R, Murphy MJ, et al. Stereotactic radiosurgery for lung tumours: preliminary report of a phase I trial. *Ann Thorac Surg* 2003;**75**:1097–101.
7. Onimaru R, Shirato H, Shimizu S, et al. Tolerance of organs at risk in small-volume, hypofractionated, image-guided radiotherapy for primary and metastatic lung cancers. *Int J Radiat Oncol Biol Phys* 2003;**56**:126–35.
8. Lee SW, Choi EK, Park HJ, et al. Stereotactic body frame based fractionated radiosurgery on consecutive days for primary or metastatic tumours in the lung. *Lung Cancer* 2003;**40**:309–15.
9. Wulf J, Haedinger U, Oppitz U, Thiele W, Mueller G, Flentje M. Stereotactic radiotherapy for primary lung cancer and pulmonary metastases: a noninvasive treatment approach in medically inoperable patients. *Int J Radiat Oncol Biol Phys* 2004;**60**:186–96.
10. Hof H, Hoess A, Oetzel D, Debus J, Herfarth K. Stereotactic single-dose radiotherapy of lung metastases. *Strahlenther Onkol* 2007;**183**:673–8.
11. Norihisa Y, Nagata Y, Takayama K, et al. Stereotactic body radiotherapy for oligometastatic lung tumours. *Int J Radiat Oncol Biol Phys* 2008;**72**:398–403.
12. Rusthoven KE, Kavanagh BD, Burri SH, et al. Multi-institutional phase I/II trial of stereotactic body radiation therapy for lung metastases. *J Clin Oncol* 2009;**27**:1579–84.
13. Ricardi U, Filippi AR, Guarneri A, et al. Stereotactic body radiation therapy for lung metastases. *Lung Cancer* 2012;**75**:77–81.
14. Widder J, Klinkenberg TJ, Ubbels JF, Wiegman EM, Groen HJ, Langendijk JA. Pulmonary oligometastases: metastasectomy or stereotactic ablative radiotherapy? *Radiother Oncol* 2013;**107**:409–13.
15. De Jaeger K, Hoogeman MS, Engelsman M, et al. Incorporating an improved dose-calculation algorithm in conformal radiotherapy of lung cancer: re-evaluation of dose in normal lung tissue. *Radiother Oncol* 2003;**69**:1–10.
16. Chetty IJ, et al. On the correlation of dose–volume response using Monte Carlo dose calculation in conformal radiation therapy of lung cancer. In: *Proceedings of the 14th ICCR*. 2004. p. 457–60.
17. Lindsay PE, El Naqa I, Hope AJ, et al. Retrospective Monte Carlo dose calculations with limited beam weight information. *Med Phys* 2007;**34**:334–46.
18. Wurm RE, Gum F, Erbel S, et al. Image guided respiratory gated hypofractionated Stereotactic Body Radiation Therapy (H-SBRT) for liver and lung tumours: initial experience. *Acta Oncol* 2006;**45**(7):881–9.
19. Radiation Therapy Oncology Group. RTOG 0813. Seamless phase I/II study of stereotactic lung radiotherapy (SBRT) for early stage, centrally located. In: *Non-Small cell lung cancer (NSCLC) in medically inoperable patients*. Philadelphia, PA: RTOG; 2009.
20. Radiation Therapy Oncology Group. *RTOG 0915. A randomized phase II study comparing 2 stereotactic body radiation therapy (SBRT) Schedules for medically inoperable patients with stage I peripheral non-small cell lung cancer*. Philadelphia, PA: RTOG; 2009.

21. Keall PJ, Mageras GS, Balter JM, et al. The management of respiratory motion in radiation oncology report of AAPM Task Group 76. *Med Phys* 2006;**33**:3874–900.
22. Rubio C, Hernando-Requejo O, Zucca Aparicio D, et al. Image guided SBRT for multiple liver metastases with ExacTrac® Adaptive Gating. *Reports Pract Oncol Radiother* 2017;**22**:150–7.
23. Li R, Mok E, Chang DT, et al. Intrafraction verification of gated RapidArc by using beam-level kilovoltage X-ray images. *Int J Radiat Oncol Biol Phys* 2012;**83**:e709–15.
24. Patel A, Khalsa B, Lord B, Sandrasegaran K, Lall C. Planting the seeds of success: CT-guided gold seed fiducial marker placement to guide robotic radiosurgery. *J Med Imaging Radiat Oncol* 2013;**57**:207–11.
25. Bhagat N, Fidelman N, Durack JC, et al. Complications associated with the percutaneous insertion of fiducial markers in the thorax. *Cardiovasc Intervent Radiol* 2010;**33**:1186–91.
26. Kothary N, Heit JJ, Louie JD, et al. Safety and efficacy of percutaneous fiducial marker implantation for image-guided radiation therapy. *J Vasc Interv Radiol* 2009;**20**:235–9.
27. Guckenberger M, Meyer J, Wilbert J, Baier K, Sauer O, Flentje M. Precision of image-guided radiotherapy (IGRT) in six degrees of freedom and limitations in clinical practice. *Strahlenther Onkol* 2007;**183**:307–13.
28. Berbeco RI, Nishioka S, Shirato H, Chen GTY, Jiang SB. Residual motion of lung tumours in gated radiotherapy with external respiratory surrogates. *Phys Med Biol* 2005;**50**:3655–67.
29. International Commission on Radiation Units and Measurements. *ICRU Report 62. Prescribing, recording and reporting photon beam therapy (supplement to ICRU Report 50)*. Bethesda, MD: ICRU; 1999.
30. Fippel M, Haryanto F, Dohm O, Nüsslin F, Kriesen S. A virtual photon energy fluence model for Monte Carlo dose calculation. *Med Phys* 2003;**30**:301–11.
31. Fippel M. Fast Monte Carlo dose calculations for photon beams based on the VMC electron algorithm. *Med Phys* 1999;**26**:1466–75.
32. Kawrakow I, Fippel M, Friedrich K. 3D electron dose calculations using a Voxel based Monte Carlo algorithm (VMC). *Med Phys* 1996;**23**:445–57.
33. Fippel M. Efficient particle transport simulation through beam modulating devices for Monte Carlo treatment planning. *Med Phys* 2004;**31**:1235–41.
34. Kawrakow I, Fippel M. Investigation of variance reduction techniques for Monte Carlo photon dose calculations using XVMC. *Phys Med Biol* 2000;**45**:2163–83.
35. Fippel M, Kawrakow I, Friedrich K. Electron beam dose calculations with the VMC algorithm and the verification data of the NCI working group. *Phys Med Biol* 1997;**42**: 501–20.
36. Fippel M, Laub W, Huber B, Nüsslin F. Experimental investigation of a fast Monte Carlo photon beam dose calculation algorithm. *Phys Med Biol* 1999;**44**:3039–54.
37. Siebers JV, Keall PJ, Nahum AE, Mohan R. Converting absorbed dose to medium to absorbed dose to water for Monte Carlo based photon beam dose calculations. *Phys Med Biol* 2000;**45**:983–95.
38. Sullivan Pepe M. *The statistical evaluation of medical tests for classification and prediction*. New York, NY: Oxford University Press; 2003.
39. Kallman P, Agren A, Brahme A. Tumour and normal tissue responses to fractionated non-uniform dose delivery. *Int J Radiat Biol* 1992;**62**:249–62.
40. Kaplan EL, Meier P. Nonparametric estimation from incomplete observations. *J Am Stat Assoc* 1958;**53**:457–81.
41. Das IJ, Ding GX, Ahnesjö A. Small fields: non-equilibrium radiation dosimetry. *Med Phys* 2008;**35**:206–15.
42. Haedinger U, Krieger T, Flentje M, Wulf J. Influence of calculation model on dose distribution in stereotactic radiotherapy for pulmonary targets. *Int J Radiat Oncol Biol Phys* 2005;**61**:239–49.
43. Miura H, Masai N, Oh RJ, et al. Clinical introduction of Monte Carlo treatment planning for lung stereotactic body radiotherapy. *J Appl Clin Med Phys* 2014;**15**:38–46.
44. Zhuang T, Djemil T, Qi P, et al. Dose calculation differences between Monte Carlo and pencil beam depend on the tumour location and volumes for lung stereotactic ablative body radiation therapy. *J Appl Clin Med Phys* 2013;**14**:38–51.
45. Chen H, Lohr F, Fritz P, et al. Stereotactic, single-dose irradiation of lung tumours: a comparison of absolute dose and dose distribution between pencil beam and Monte Carlo algorithms based on actual patient CT scans. *Int J Radiat Oncol Biol Phys* 2010;**78**:955–63.
46. Pokhrel D, Badkul R, Jiang H, et al. Dosimetric evaluation of centrally located lung tumours: a Monte Carlo (MC) study of lung SBRT planning [abstract]. *Med Phys* 2014;**41**:167.
47. Ojala JJ, Kapanen MK, Hyödynmaa SJ, Wigren TK, Pitkänen MA. Performance of dose algorithms for three generations in lung SBRT: comparison with full Monte Carlo-based dose distributions. *J Appl Clin Med Phys* 2014;**15**:4–18.
48. Timmerman RD, Papiez L, McGarry R. Extracranial stereotactic radioablation: results of a phase I study in medically inoperable stage I non-small cell lung cancer. *Chest* 2003;**124**:1946–55.
49. Xiao Y, Papiez L, Paulus R, et al. Dosimetric evaluation of heterogeneity corrections for RTOG 0236 stereotactic body radiotherapy of inoperable stage I-II non-small-cell lung cancer. *Int J Radiat Oncol Biol Phys* 2009;**73**:1235–42.
50. Radiation Therapy Oncology Group. *RTOG 0236. A phase II trial of stereotactic body radiation therapy (SBRT) in the treatment of patients with medically inoperable stage I/II non-small cell lung cancer*. Philadelphia, PA: RTOG; 2006.
51. Guckenberger M, Wilbert J, Krieger T, et al. Four-dimensional treatment planning for stereotactic body radiotherapy. *Int J Radiat Oncol Biol Phys* 2007;**69**:276–85.
52. Guckenberger M, Wulf J, Mueller G, et al. Dose–response relationship for image-guided stereotactic body radiotherapy of pulmonary tumours: relevance of 4D dose calculation. *Int J Radiat Oncol Biol Phys* 2009;**74**:47–54.
53. Onishi H, Shirato H, Nagata Y, et al. Hypofractionated stereotactic radiotherapy (HypoFXSRT) for stage I non-small cell lung cancer: updated results of 257 patients in a Japanese multi-institutional study. *J Thorac Oncol* 2007;**2**:S94–100.
54. Latifi K, Oliver J, Baker R, et al. Study of 201 non-small cell lung cancer patients given stereotactic ablative radiation therapy shows local control dependence on dose calculation algorithm. *Int J Radiat Oncol Biol Phys* 2014;**88**:1108–13.
55. Chetty IJ, Curran B, Cygler JE, et al. Report of the AAPM TG 105 Issues associated with clinical implementation of Monte Carlo-based photon and electron external beam treatment planning. *Med Phys* 2007;**34**:4818–53.